Density functional theory of crystal-fluid interfaces and surface melting

R. Ohnesorge, H. Löwen, and H. Wagner
Sektion Physik der Universität München, Theresienstrasse 37, D-80333 München, Germany
(Received 24 May 1994)

The equilibrium structure of various crystal-fluid interfaces in hard-sphere and Lennard-Jones systems is investigated by a density functional approach based on a weighted density approximation which yields reliable bulk phase diagrams. The practically *free* minimization of the free energy is achieved. As a result the interfaces between the hard-sphere fluid and the fcc hard-sphere crystal are found to have a width of typically seven hard-sphere diameters. A comparison with previous constrained variational calculations demonstrates that free minimization is indispensable to obtain reliable values for the surface tension. In accordance with recent computer simulations we also find complete wetting of a hard structureless planar wall by the hard-sphere crystal at crystal-fluid coexistence. Finally, the fcc-crystal–gas interface of a Lennard-Jones system exhibits complete surface melting near the triple point for different surface orientations. The width of the interfacial quasiliquid layer depends significantly on temperature and on surface orientation.

PACS number(s): 68.45.−v, 64.70.−p, 68.35.−p

I. INTRODUCTION

The interface between two coexisting phases in thermodynamic equilibrium normally has a microscopic width and is characterized by an interfacial tension measuring the free energy cost per unit area in creating it. If one of the two coexisting phases is crystalline, the surface tension of a planar interface is anisotropic [1] and expected to be smaller for densely packed planes than for looser packed ones. This orientational variation of the interfacial free energy is particularly important in determining the equilibrium crystal shape [2].

A similar situation arises when a solid or fluid is confined by an inert hard wall. Acting as an external inhomogeneity on the bulk system, the wall induces an interface of microscopic width with a characteristic wall tension. If the bulk system is close to coexistence, the balance between bulk and surface free energies may drive surface phase transitions such as the wetting of the wall by the metastable bulk phase [3]. In the case of complete wetting the width of the wetting layer diverges at coexistence. Similarly, an interface between two coexisting phases near a triple point may be wetted by the incipient phase. A prominent example is "surface melting" of a solid in coexistence with its vapor phase. When the triple point is approached along the sublimation line, a quasiliquid layer may be formed at the solid surface which grows steadily towards a bulk liquid phase, provided the interfacial wetting is complete.

In the last decade, the study of solid-fluid interfaces has advanced considerably on the experimental as well as on the theoretical side; for recent reviews see [4] (experiments) and [5] (theory). However, as far as *microscopic theories* are concerned where the only input should be the interparticle interaction [6], the understanding of interfacial structure is still limited even for very simple systems such as hard spheres or noble-gas-like models with pairwise Lennard-Jones forces. The problem is that one needs an accurate microscopic theory of bulk melting before interfacial problems can be addressed. Recently, liquid-based density functional methods have been developed [5–8] where freezing is viewed as a condensation of liquid density modes. When applied to the hard-sphere fluid, the bulk phase diagram turned out to be in satisfactory agreement with the results of computer simulation. In this paper, we employ the density functional approach to study the equilibrium density distribution of various crystal-fluid interfaces of hard-sphere and Lennard-Jones systems. In particular, we use the weighted-density approximation (WDA), originally introduced by Curtin and Ashcroft [9,10].

Previous similar studies of interfaces frequently invoke the square-gradient approximation for slowly varying order parameter profiles, which leads to a van der Waals or Landau-type scheme where the parameters are obtained microscopically from the density functional theory [11,12]. With this strategy the structure of both the hard-sphere crystal-fluid interface [13] and the crystal-gas Lennard-Jones surface near the triple point [14] have been investigated in terms of order parameter profiles. Only few attempts have been made to avoid the square-gradient approximation and to perform a direct minimization of the free energy functional. Curtin [15,16] applied the WDA to the hard-sphere and Lennard-Jones crystal-liquid interfaces with a density profile described solely by two parameters. Cherepanova and Stekolnikov [17] examined surface melting of a Lennard-Jones system near the triple point [18] within a simplified WDA proposed by Tarazona [19].

Functional such as the generalized effective liquid approximation (GELA) [20], the modified weighted-density approximation (MWDA) [21], and the hybrid weighted-density approximation (HWDA) [22] are computationally less demanding than the WDA but cannot be employed to investigate crystal-fluid interfaces since these approximations are based on a globally averaged density which is not well defined in the case of systems with two semi-infinite bulk phases. As an interpolation between the

MWDA and the WDA, the planar-averaged weighted-density approximation (PWDA) was recently introduced by Marr and Gast [23] and applied to explore crystal-fluid hard-sphere interfaces as well as the solid-gas and solid-liquid interface of Lennard-Jones systems within Curtin's two-parameter ansatz.

Our present work differs from the previous ones in one major respect: We performed a practically *free* minimization of the WDA functional. We treat hard-sphere crystal-fluid interfaces with different orientations and the hard-sphere crystal in contact with a hard wall as well as surface melting of a Lennard-Jones system. The fcc-crystalline–fluid surface tension of hard spheres is reduced by a factor of 2 as compared with the results of Curtin [15] and with those of Marr and Gast [23]. We also find that a hard wall is completely wetted by a hard-sphere crystal at solid-fluid coexistence, in accordance with recent molecular-dynamics simulations of Courtemanche and co-workers [24]. Finally, a Lennard-Jones fcc crystal undergoes complete surface melting near the triple point for (111), (100), and (110) orientation. The wetting layer displays a rich structure involving residual crystallinities and a density oscillation induced by the vapor side of the interface.

The presentation is arranged as follows. In Sec. II we introduce the density functional approach and discuss the WDA. The numerical procedure applied to minimize the free energy functional is summarized in Sec. III. Results for the different hard-sphere crystal-fluid interfaces are given in Sec. IV and for the surface melting in Lennard-Jones interfaces in Sec. V. We conclude in Sec. VI. A preliminary account of this work was published elsewhere [25].

II. DENSITY FUNCTIONAL THEORY

In the density functional approach the central quantity is the grand canonical free energy functional $\Omega[\rho]$ of an inhomogeneous system with local density $\rho(\mathbf{r})$, temperature T, and chemical potential μ. The basic variational principle [26] establishes the existence of an excess free energy functional $\mathcal{F}_{\rm exc}[\rho]$ such that the equilibrium density *minimizes* the grand canonical free energy functional,

$$\Omega[\rho]=\mathcal{F}_{\rm exc}[\rho]+\int d^3r\,\rho(\mathbf{r})(V_{\rm ext}(\mathbf{r})-\mu+k_BT\{\ln[\Lambda^3\rho(\mathbf{r})]-1\}) . \quad (1)$$

The minimum of $\Omega[\rho]$ equals the grand canonical free energy in thermal equilibrium. In Eq. (1), Λ denotes the thermal wavelength and $V_{\rm ext}(\mathbf{r})$ is an external potential induced, for instance, by a wall. In general, the explicit form of $\mathcal{F}_{\rm exc}[\rho]$ is not known and one has to rely on approximations. We shall proceed with the weighted-density approximation for hard spheres combined with a perturbative treatment of the Lennard-Jones potential.

A. WDA for hard spheres

The excluded volume interaction for hard spheres is given by the pair potential

$$V_{\rm HS}(r)=\begin{cases}0 & \text{for } r\geq\sigma\\ \infty & \text{for } r<\sigma\end{cases} , \quad (2)$$

with σ denoting the diameter of the spheres.

In the original WDA [9], the excess free energy functional for hard spheres is assumed to be of the form

$$\mathcal{F}_{\rm exc}[\rho]=\int d^3r\,\rho(\mathbf{r})\Psi(\bar\rho(\mathbf{r})) , \quad (3)$$

where $\Psi(\rho)$ is the excess free energy per particle for a homogeneous density; the weighted density $\bar\rho(\mathbf{r})$ is determined implicitly by

$$\bar\rho(\mathbf{r})=\int d^3r'\,w(|\mathbf{r}-\mathbf{r}'|,\bar\rho(\mathbf{r}))\rho(\mathbf{r}') . \quad (4)$$

The weight function $w(r,\rho)$ is normalized and chosen in such a way that the liquid structure factor $S(k,\rho)$ is reproduced by the functional $\mathcal{F}_{\rm exc}[\rho]$ in the limit of a uniform density. For $\Psi(\rho)$ and $S(k,\rho)$ we adopt the analytical Percus-Yevick expressions [27].

In order to simplify the numerical computation of the weighted density $\bar\rho(\mathbf{r})$ via Eq. (4), we introduce a further approximation. Since by construction the weight function $w(r,\rho)$ depends smoothly on the density ρ, it may be expanded in a Taylor series around a fixed reference density ρ^*. We choose $\rho^*\sigma^3=0.5$, lying roughly between the ideal gas limit and the solid density at freezing, and truncate the Taylor expansion after the quadratic term. Hence we set

$$w(r,\rho)\approx\sum_{n=0}^{2}\frac{1}{n!}[\rho-\rho^*]^n\frac{\partial^n}{\partial\rho^n}w(r,\rho^*) . \quad (5)$$

A comparison of $w(r,\rho)$ obtained from (5) with the solution of the complete WDA reveals that the differences are negligibly small for physically relevant densities near ρ^*. Figure 1 demonstrates that the density-expanded weight

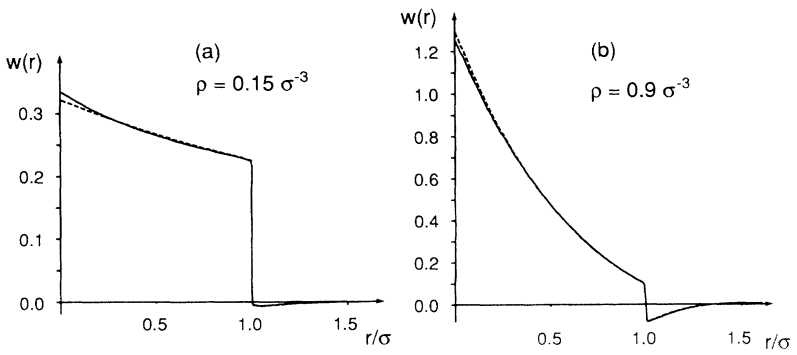

FIG. 1. Weight function $w(r)$ of the WDA vs reduced distance r/σ for $\rho\sigma^3=0.15$ and 0.9. The results from the full WDA (solid lines) practically coincide with the dashed lines which correspond to the quadratic expansion of $w(r,\rho)$ around $\rho^*=0.5\sigma^{-3}$.

TABLE I. Coexisting liquid and fcc-crystal densities, $\rho_f\sigma^3$ and $\rho_c\sigma^3$, for a hard-sphere system obtained with different methods: computer simulation [47], the density-expanded WDA, and the original WDA (from [9,21]). The liquid free energy Ψ was obtained using either the Percus-Yevick (PY) or the Carnahan-Starling (CS) equation of state, and the crystal density parametrization was either Gaussian or free. The Lindemann parameter L of the coexisting crystal [29] is also given.

Method	Expanded	Ψ	Parametrization	$\rho_f\sigma^3$	$\rho_c\sigma^3$	L
simulation				0.943	1.041	0.136
WDA	no	CS	Gaussian	0.916	1.045	0.093
WDA	yes	CS	Gaussian	0.916	1.044	0.097
WDA	yes	PY	Gaussian	0.880	1.017	0.105
WDA	yes	PY	free	0.853	1.044	0.160

function (5) practically coincides with the nontruncated $w(r,\rho)$ even for low densities $\rho\sigma^3=0.15$, as well as for $\rho\sigma^3=0.9$, a density near freezing. Consequently, the expansion (5) is justified. Equation (4) can now be solved analytically for $\bar{\rho}(\mathbf{r})$ yielding a unique physically relevant root [28].

During the minimization of the free energy functional, overlapping hard-sphere configurations must be excluded [14]. In terms of the inhomogeneous density field $\rho(\mathbf{r})$ this constraint means that

$$\int d^3r'\Theta\left[\frac{\sigma}{2}-|\mathbf{r}-\mathbf{r}'|\right]\rho(\mathbf{r}')\leq 1 \tag{6}$$

has to be satisfied at any point $\mathbf{r}$; here $\Theta(x)$ denotes the unit step function. The exact but unavailable free energy functional respects this relation automatically, of course. Here, however, this constraint has to be implemented explicitly, since the WDA as well as the other known approximation schemes have no internal mechanism to exclude such unphysical configurations. Except for this constraint the minimization within the subspace of fcc-lattice-periodic functions will be practically free, including also a variation of the lattice constant. Details of the numerical procedure to obtain the bulk phase diagram are given in Sec. III. The deviations of the equilibrium density field from the usual Gaussian peak form were previously discussed in detail [29] and turned out to be very small. However, the anisotropy of the solid density distribution deviates qualitatively from the simulation results.

Bulk freezing data are collected in Table I together with those from other approximation schemes. The Percus-Yevick and the more accurate Carnahan-Starling expressions for the liquid free energy yield different results for the coexisting liquid and solid densities. Since the treatment of interfaces requires a unified description of coexisting bulk phases we adopt the Percus-Yevick form exclusively. By the free minimization the coexisting densities are also changed slightly in comparison with the usual Gaussian parametrization. We checked that the results are not affected by the quadratic density expansion of $w(r,\rho)$. Irrespective of the approximate scheme employed, the coexisting densities are found to be in reasonable agreement with the computer simulation results.

B. Density functional for the Lennard-Jones system

We treat the Lennard-Jones (LJ) potential

$$V_{\mathrm{LJ}}(r)=4\epsilon\left[\left[\frac{\bar{\sigma}}{r}\right]^{12}-\left[\frac{\bar{\sigma}}{r}\right]^{6}\right] \tag{7}$$

within hard-sphere perturbation theory [10]. In the first step, made for numerical reasons, we follow Foiles and Ashcroft [30] and approximate the LJ potential by a sum of two Yukawa potentials,

$$\begin{aligned}V_{\mathrm{LJ}}(r)&\approx V_{\mathrm{FA}}(r)\\&=\epsilon E\frac{\bar{\sigma}}{r}\left\{\exp\left[-a\left[\frac{r}{\bar{\sigma}}-1\right]\right]\right.\\&\qquad\left.-\exp\left[-b\left[\frac{r}{\bar{\sigma}}-1\right]\right]\right\},\end{aligned} \tag{8}$$

with $E=2.019\,869$, $a=14.734\,18$, $b=2.679\,24$. In the next step the potential $V_{\mathrm{FA}}(r)$ is separated into a repulsive and an attractive part, $V_{\mathrm{FA}}(r)=V_r(r)+V_a(r)$, according to the prescription of Weeks, Chandler, and Anderson [31]

$$V_a(r)=\begin{cases}V_{\mathrm{FA}}(r) & \text{for } r\geq 2^{1/6}\bar{\sigma}\\ V_{\mathrm{FA}}(2^{1/6}\bar{\sigma}) & \text{for } r<2^{1/6}\bar{\sigma}\ .\end{cases} \tag{9}$$

The repulsive core is now replaced by an effective temperature-dependent hard-sphere diameter $\sigma(T)$ obtained from the Barker-Henderson formula [32]

$$\sigma(T)=\int_0^\infty dr\{1-\exp[-V_r(r)/k_BT]\}\ . \tag{10}$$

In the last step the free energy functional is split into a part arising from the repulsive core and the contribution from the attraction. For the first part, denoted by $\Omega_{\mathrm{WDA}}[\rho]$, we substitute the WDA expression for hard spheres with diameter $\sigma(T)$. The attraction is treated in a mean field fashion. However, there is apparently no unique way to do this. The criteria for our procedure are first that the free energy of the uniform liquid should be reproduced and second that the solid and the liquid are treated on the same footing, which is necessary for a consistent description of crystal-fluid interfaces. With these requirements in mind, we are led to the following ansatz:

$$\Omega[\rho]=\Omega_{\mathrm{WDA}}[\rho]+\int d^3r\,\tilde{\rho}(\mathbf{r})[\Psi_{\mathrm{LJ}}(\tilde{\rho}(\mathbf{r}))-\Psi_{\mathrm{HS}}(\tilde{\rho}(\mathbf{r}))]$$
$$+\frac{1}{2}\int d^3r\int d^3r'[\rho(\mathbf{r})-\tilde{\rho}(\mathbf{r})][\rho(\mathbf{r}')-\tilde{\rho}(\mathbf{r}')]$$
$$\times V_a(|\mathbf{r}-\mathbf{r}'|)\Theta\left(|\mathbf{r}-\mathbf{r}'|-\frac{r_{\mathrm{NN}}}{2}\right), \tag{11}$$

where r_{NN} is the nearest neighbor distance in the bulk crystal. Here we follow with a minor modification (see below) arguments put forward by Curtin and Ashcroft [10] and include a step function $\Theta(r)$ in the attractive interaction to mimic the correlation "hole" for $r<r_{NN}/2$ in the pair distribution function which prevents self-interaction [18].

If $\tilde{\rho}(\mathbf{r})$ is replaced by the mean density of the crystal ρ_c, then Eq. (11) reduces to the corresponding expression given in Ref. [10]. However, in dealing with interfaces we must avoid globally averaged densities. Therefore we introduce an additional locally weighted density,

$$\tilde{\rho}(\mathbf{r})=\int d^3r'\rho(\mathbf{r}')\bar{w}(|\mathbf{r}-\mathbf{r}'|)\ . \tag{12}$$

The normalized linear weight function $\bar{w}(r)$ is chosen such that rapid modulations of $\tilde{\rho}(\mathbf{r})$ in the crystalline phase are suppressed. Accordingly, we set

$$\bar{w}(r)=\frac{24}{\pi\sigma(T)^3}\left[1-\frac{r}{\sigma(T)}\right]\Theta(\sigma(T)-r)\ . \tag{13}$$

Since $\bar{w}(r)$ is normalized, the last term in (11) vanishes in the homogeneous liquid. Consequently, the excess free energies per particle, $\Psi_{\mathrm{HS}}(\rho)$ and $\Psi_{\mathrm{LJ}}(\rho)$, of the hard sphere and the LJ liquid are reproduced in the uniform state. As for $\Psi_{\mathrm{HS}}(\rho)$ we take the analytic Percus-Yevick expression, and we employ the results of Verlet and Weis [33] for $\Psi_{\mathrm{LJ}}(\rho)$.

The bulk phase diagram is displayed in Fig. 2. Compared with the results from computer simulation [34] with a truncated LJ potential, the overall agreement is satisfactory. The triple point is at $T_T=0.75\epsilon/k_B$ in the WDA; the simulation result is $T_T=0.68\pm0.02\epsilon/k_B$. In comparison with the usual Gaussian ansatz the free minimization in the solid phase shifts the solid-liquid coexistence curve to smaller densities.

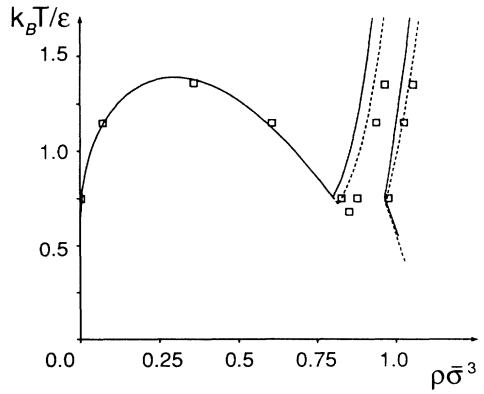

FIG. 2. Bulk phase diagram for a Lennard-Jones system obtained from density functional theory with free minimization of the solid density (solid line) and the Gaussian parametrization (dashed line). Squares denote simulation data for a truncated LJ potential from Ref. [34].

III. NUMERICAL IMPLEMENTATION

Let us consider a planar crystal-fluid interface with surface normal in z direction in a finite rectangular slab with periodic boundary conditions in each direction. The widths L_x and L_y of the slab in x and y direction are chosen to be a few lattice spacings. In contrast, the length L_z of the slab in z direction must be sufficiently large to eliminate the interaction of periodically repeated interfaces. Here, the short range of the forces enters crucially. Our choice for the length L_z is typically between 17σ and 26σ.

The density is parametrized in terms of its Fourier coefficients,

$$\rho(\mathbf{r})=\sum_{\mathbf{G}}\rho_{\mathbf{G}}\exp(i\mathbf{G}\cdot\mathbf{r})\ , \tag{14}$$

where $\mathbf{G}=(G_x,G_y,G_z)$ are the reciprocal lattice vectors of the periodic slab. The infinite sum is truncated for $|G_x|>\pi N_x/L_x$, $|G_y|>\pi N_y/L_y$, and $|G_z|>\pi N_z/L_z$, where N_x, N_y, and N_z are integers such that the ratios L_x/N_x, L_y/N_y, and L_z/N_z are roughly equal. This truncation provides in real space a set of equidistant grid points where the density field is defined. The distances between two neighboring grid points, L_x/N_x, L_y/N_y, and L_z/N_z, are typically of the order of $\sigma/40$. Hence even the rapid density variations in the solid phase can be resolved with high accuracy. For an interface calculation, the total number of variational parameters $\{\rho_{\mathbf{G}}\}$ is of the order of $N=N_xN_yN_z=2\times10^6$, which is at the storage limit of present-day computers. Because of symmetry, this number may be reduced to maximally 0.5×10^6 *independent* variables. Minimization is also performed with respect to the system size L_x, L_y, and L_z.

The convolution integrals in the density functional are evaluated in Fourier space whereas the local nonlinear part of the functional is computed in real space. Efficient fast-Fourier-transformation (FFT) routines are then used to switch between real and reciprocal space. We introduce free energy penalties in order to eliminate overlapping hard-sphere configurations, as described in Ref. [14]. By employing the Fourier representation of the density, Eq. (14), the gradient of the free energy functional with respect to the N variational parameters $\{\rho_{\mathbf{G}}\}$ can be calculated with one FFT operation whereby the computational effort is drastically reduced.

There is a variety of methods available for minimization in a high-dimensional parameter space starting from a given point, provided the functional and its multidimensional gradient are known. For our purpose, we found a procedure, which might be called *simulated quenching,* very efficient and in general superior to a conjugated gradient scheme. For an outline of the method, which is inspired by *simulated annealing,* let us consider a fictitious particle in multiparameter space

$\{\Gamma_i\} \equiv \{\rho_G, L_x, L_y, L_z\}$ with a mass m which moves according to Newton's second law where the gradient $\partial F/\partial \Gamma_i$ acts as force [35]. Thereby, trajectories $\{\Gamma_i(t)\}$ with a time parameter t are generated. The process starts from an initial density profile at $t=0$ with zero velocity $\{\dot{\Gamma}_i(0)\}$. When the kinetic energy reaches a maximum we stop the particle ("quenching") and then start the process again. Newton's equations are integrated using a finite time-step method. On a Cray YMP one time step consumes a CPU time of about 15 s. Depending on the initial density profile, the minimization process takes about 10^3-10^4 time steps. The interfacial tension is obtained after separation of the minimal free energy functional into a bulk and a surface part.

IV. HARD-SPHERE INTERFACES

A. Crystal-fluid interface

We first consider a planar hard-sphere fcc-crystal–fluid interface at coexistence. The structure of the interface is conveniently characterized by the laterally integrated particle number density, defined by

$$\rho^{\perp}(z) = \frac{1}{A} \int_A dx\, dy\, \rho(\mathbf{r}) , \tag{15}$$

with the surface area A. Results for the profile $\rho^{\perp}(z)$ are shown in Fig. 3 for three orientations within an interval of length $L_z/2$. The width of the interfaces is typically 7σ, being significantly larger than Curtin's results obtained with a two-parameter ansatz [15]. This widening is due to smectic-type density peaks on the liquid side of the interface, with a separation slightly larger than that of the crystalline layers. A measure of the lateral density modulations in the planes perpendicular to the z direction is given by the minimal density

$$\rho_m(z) = \min_{(x,y)} \rho(\mathbf{r}) , \tag{16}$$

which is practically zero in the solid phase and equals the bulk density in the fluid phase. Inspection of $\rho_m(z)$ starting from the fluid phase reveals that the longitudinal density wave in the (111) interface evolves before the lateral modulation sets in, whereas in the (110) interface the situation is reversed. The density parametrization permits a relaxation of the crystal in z direction. Nevertheless the observed enhancement of the lattice constant towards the surface is at most 2%.

The values of the crystal-fluid surface tensions turn out to be $\gamma_{cf}^{(100)} = 0.35 k_B T/\sigma^2$, $\gamma_{cf}^{(110)} = 0.30 k_B T/\sigma^2$, and $\gamma_{cf}^{(111)} = 0.26 k_B T/\sigma^2$. Unfortunately, there are apparently no computer simulation results for these surface tensions to compare with. Within the WDA, Curtin [15,16] obtained $\gamma_{cf}^{(100)} = 0.66 k_B T/\sigma^2$ and $\gamma_{cf}^{(111)} = 0.63 k_B T/\sigma^2$. Hence the free minimization reduces the surface tension roughly by a factor of 2.

B. Solid-liquid coexistence of hard spheres near a hard wall

The problem of a liquid in the vicinity of a rigid wall received much attention [36,22] and has become a standard test for any approximation scheme devised to deal with strongly inhomogeneous systems. On the other hand, the effect of a wall on solid and liquid phases of hard spheres in coexistence has not yet been examined within a density functional approach. In particular, the question is whether a wall is wetted by the liquid or by the solid. Recent molecular-dynamics simulations [24] indicate that the planar wall prefers the crystalline phase and we confirm this finding with the following results.

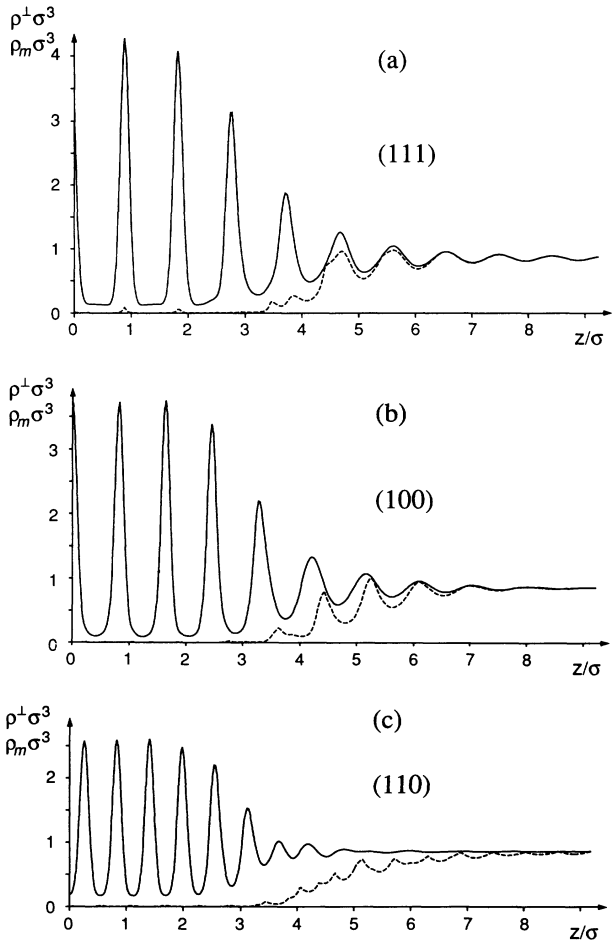

FIG. 3. Parallel-integrated density $\rho^{\perp}(z)$ (full curves) and minimal density $\rho_m(z)$ (dashed curves) vs z/σ for a hard-sphere crystal-fluid interface obtained from the WDA. The densities are in units of σ^{-3}. (a) (111) orientation; (b) (100) orientation; (c) (110) orientation.

The density profile obtained from a freely minimized WDA functional is displayed in Fig. 4. The contact value of the density is fixed by the wall theorem [37], $\rho_W = P/k_B T$, in terms of the bulk pressure P, irrespective of whether the wetting phase is liquid or solid. The crystal density profile shown in Fig. 4(b) attains its bulk form already after two lattice distances from the wall. For the interfacial wall-crystal tension we find $\gamma_{wc}^{(111)} = -2.80 k_B T/\sigma^2$, with a negative sign since the bulk volume is defined by the location of the sphere centers [38]. The wall-fluid tension, $\gamma_{wf}^{*} = -2.50 k_B T/\sigma^2$, exceeds the wall-crystal tension by a substantial amount. Hence we conclude that the wall is indeed wetted by the

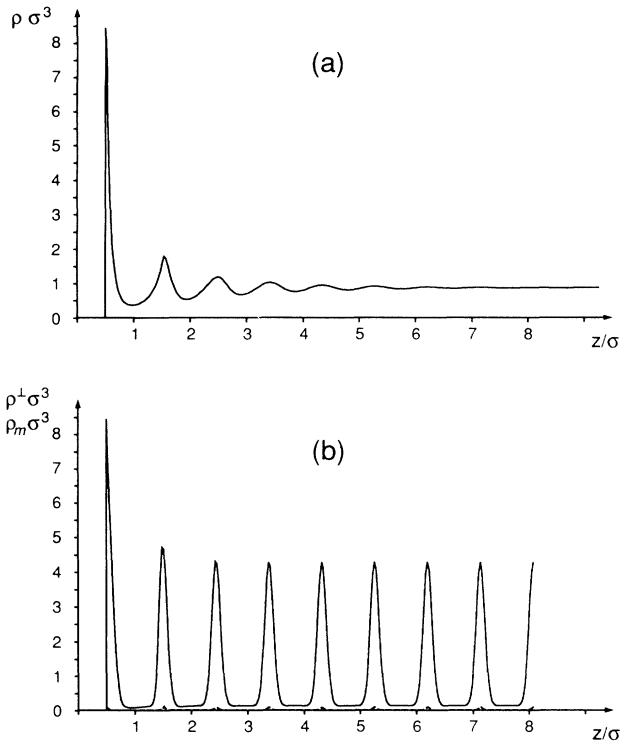

FIG. 4. Density profile of hard spheres near a hard wall located at $z=0$ at fluid-solid coexistence vs distance z/σ: (a) liquid at the wall, (b) crystal at the wall. In the latter case, the parallel-integrated density $\rho^{\perp}(z)$ (full curve) is shown for the (111) orientation while the minimal density $\rho_m(z)$ (dashed curve) practically vanishes.

solid phase with the (111) axis normal to the wall, in accordance with the simulation result. Moreover, we predict the wetting to be complete because $\gamma^{*}_{wf} > \gamma_{wc} + \gamma_{cf}$.

V. SURFACE MEETING OF A LENNARD-JONES CRYSTAL

The surface of a solid is an omnipresent defect in the crystal structure and provides a natural stage where thermal disorder can be induced without a nucleation barrier. In fact, there is ample empirical evidence that the melting process in thermal equilibrium starts definitely below the bulk triple point T_T by wetting the crystal-vapor interface with a quasiliquid film. Once this film is established, the growth law for its thickness $l(\tau)$ upon approaching the triple point, $1-T/T_T \equiv \tau \to 0$, may be inferred from a simple estimate [12] of the interfacial free energy which yields

$$l(\tau) = D \ln(\tau_0/\tau) \ . \tag{17}$$

This logarithmic growth is predicted to hold on a scale determined by the decay length of the residual crystallinity in the film. With increasing width a crossover to the power law

$$l(\tau) \propto \tau^{-1/3} \tag{18}$$

is expected when the van der Waals attraction governs the interaction between the crystal-liquid and the liquid-vapor interfaces of the thick film.

Recent experiments on surface melting have been made with rare gas crystals [39], ice [40], and lead [41,5]. The measurements with lead, in particular, confirm both growth laws (17) and (18). Surface melting of Lennard-Jones crystals has also been investigated by computer simulations [42], but the data are still inconclusive due to significant finite size effects.

Here we report on our effort to deal with the anisotropic *onset* of surface melting in Lennard-Jones crystals at finite values of the reduced temperature τ by employing density functional methods. This issue cannot be addressed with a phenomenological approach where the existence of a wetting film viewed as an undercooled liquid is taken for granted, but requires a fully microscopic theory such as outlined in Secs. II and III.

Our results for the laterally integrated density profiles of a slab are shown in Figs. 5(a)–5(e) for the (111), (110), and (100) orientations in a fcc crystal. Surface melting is visible for each orientation, with a clear anisotropy in the structure of the interface. As expected, the more loosely packed (110) and (100) planes are more disordered than the dense (111) plane. The evolution of the (110) profile from $\tau=10^{-2}$ to $\tau=10^{-4}$ is illustrated in Figs. 5(d) and 5(e) and indicates complete surface melting which is found for the (111) and (100) orientation as well. The complexity of the density distribution is illustrated by the contour plots in Fig. 6. There one can also see that the lateral order in the (110) surface is strongly anisotropic. Since we have a short-ranged interaction (8) between the particles, the growth law for the film is given by (17) without crossover to algebraic growth. Even though there is no unique definition of the width l, the prefactor D is determined by Figs. 5(c)–5(e). Figure 7 shows the temperature dependence of l. D is proportional to the slope of the interpolating line and has a value of $1.3\pm0.2\bar{\sigma}$ or approximately two layers. This compares well with a neutron experiment on methan which yields $D \approx 1.65$ layers [43].

Evans *et al.* [44] recently predicted a nonmonotonic density profile of a planar liquid-vapor interface with small-amplitude oscillations decaying towards the bulk liquid. The structure arises from packing effects due to inhomogeneities such as a steplike density variation in an interface. These arguments may also explain the shallow bump adjacent to the vapor phase seen in the $\rho^{\perp}(z)$ profile of the thick wetting layer at $\tau=10^{-4}$. The interaction of this density oscillation with those induced by the solid may affect the growth of the wetting layer as $\tau \to 0$. For the (100) orientation we observed a hysteresis effect in minimizing the density functional for increasing and decreasing temperature which hints at a discontinuous layer-by-layer growth via a first-order surface phase transition. On the other hand, the amplitude of the bump in the liquid-gas interface depends sensitively on the form of the last term in (11). Thus a quantitative analysis of this problem remains an open task.

At the triple point, the crystal-liquid surface tensions are obtained to be $\gamma_{cl}^{(111)}=0.23\epsilon/\bar{\sigma}^2$, $\gamma_{cl}^{(100)}=0.29\epsilon/\bar{\sigma}^2$, and $\gamma_{cl}^{(110)}=0.27\epsilon/\bar{\sigma}^2$. These values are in reasonable

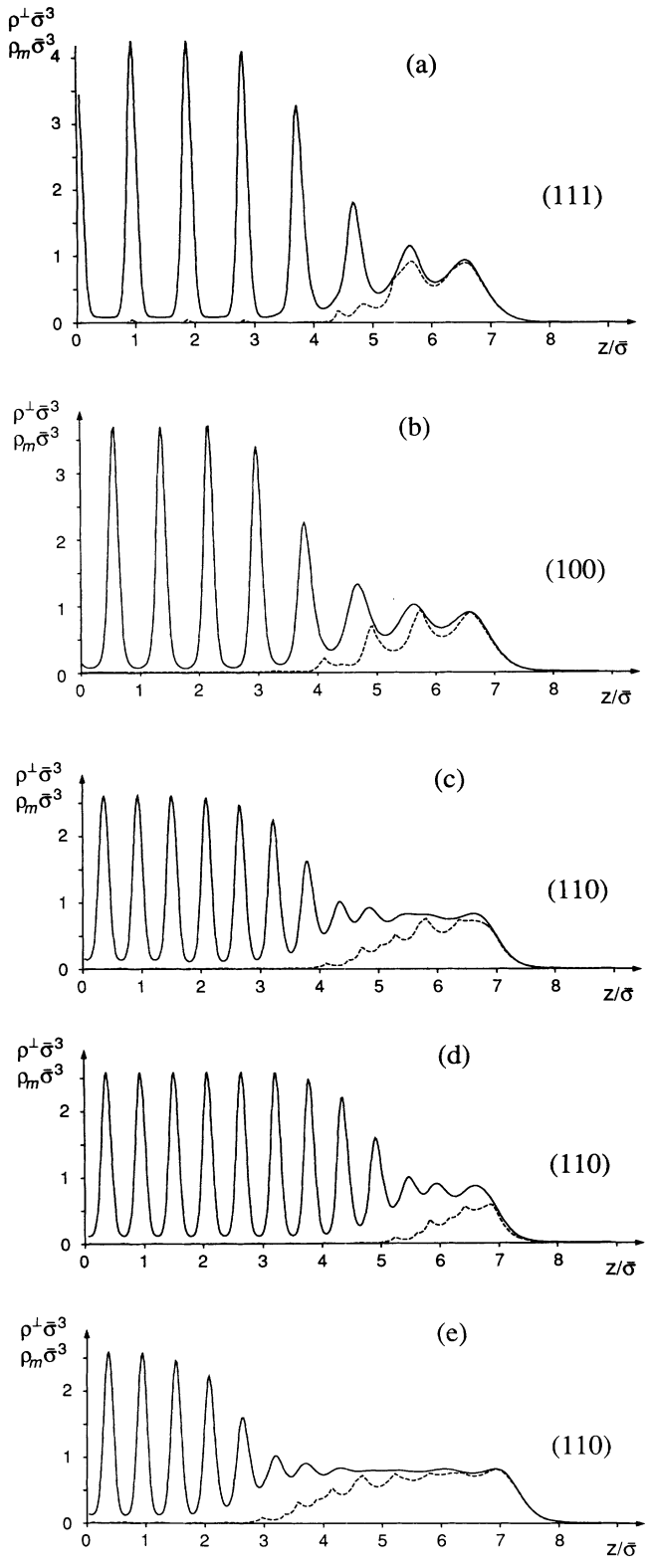

FIG. 5. Parallel-integrated density $\rho^{\perp}(z)$ vs z for a LJ system obtained from hard-sphere perturbation theory of the WDA: (a) reduced temperature $\tau=10^{-3}$ and (111) orientation; (b) reduced temperature $\tau=10^{-3}$ and (100) orientation; (c) reduced temperature $\tau=10^{-3}$ and (110) orientation; (d) reduced temperature $\tau=10^{-2}$ and (110) orientation; (e) reduced temperature $\tau=10^{-4}$ and (110) orientation.

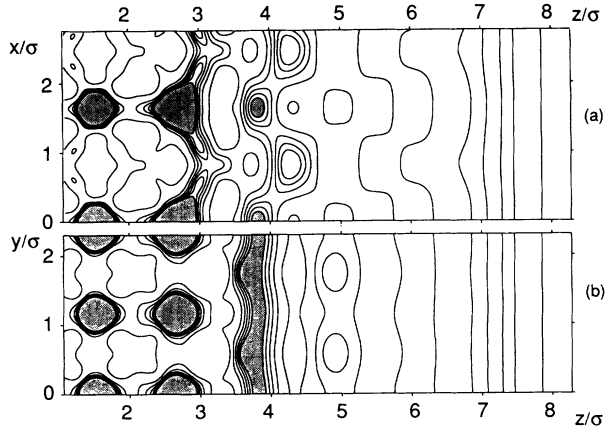

FIG. 6. (110) surface of a LJ crystal at $\tau=10^{-4}$: Contour plots of the density in a $(1\bar{1}0)$ plane (a) and a (001) plane (b). Both planes are normal to the surface and hit the lattice sites. Lines correspond to densities $\rho\sigma^3=0.05+n0.25$, $n=0,\ldots,6$. The shaded areas correspond to $\rho\sigma^3>1.55$.

agreement with the simulational data [45]: $\gamma_{cl}^{(111)}=0.35\pm0.02\epsilon/\bar{\sigma}^2$, $\gamma_{cl}^{(100)}=0.34\pm0.02\epsilon/\bar{\sigma}^2$, and $\gamma_{cl}^{(110)}=0.36\pm0.02\epsilon/\bar{\sigma}^2$. It should be mentioned that the LJ potential was truncated differently in the simulation and in our theory; the triple temperature in this simulation is only $T_T=0.61\epsilon/k_B$. A two-parameter variation [16] yields $\gamma_{sl}^{(111)}=0.43\epsilon/\bar{\sigma}^2$. Within the WDA, the liquid-gas surface tension at the triple point is $\gamma_{lg}=0.40\epsilon/\bar{\sigma}^2$ and deviates from the simulational result $\gamma_{lg}=0.8\pm0.4\epsilon/\bar{\sigma}^2$ [46]. The latter value is limited, however, by a rather large statistical error. Compared to our previous work [14] based on the square-gradient approximation, the present values of the surface tensions are significantly lower. This is not surprising since the square-gradient approximation is known to overestimate the surface tensions.

Finally we show in Fig. 8 the scattering intensity measured with evanescent x-ray scattering [4] from the sur-

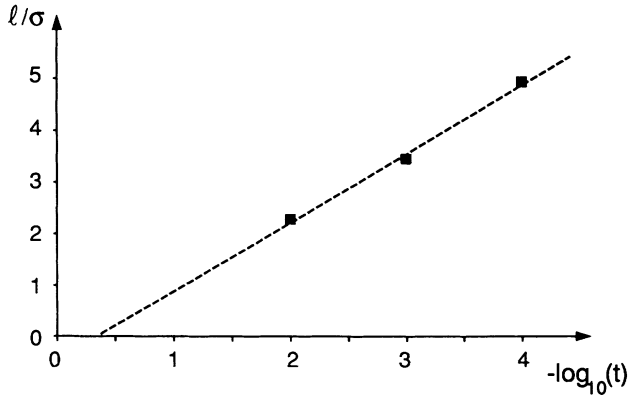

FIG. 7. Width l of the quasiliquid film in dependence of the reduced temperature t. The squares correspond to the last three profiles in Fig. 5. The dashed line is a guide to the eye.

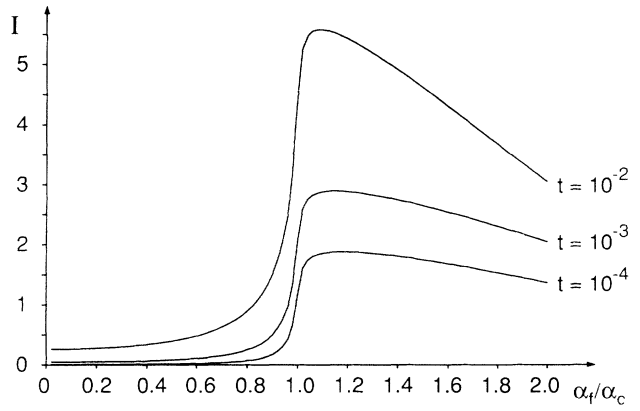

FIG. 8. Intensity: I of x rays scattered under grazing incidence from a melting LJ (110) surface at different reduced temperatures t vs angle ratio α_f/α_c. The parameters adapted to xenon are given in the text. (I in arbitrary units.)

faces displayed in Figs. 5(c)–5(e). The intensity is proportional to

$$I=\left|\int d^3r \exp\{-i[G_x x+G_y y+\kappa(z-z_0)] +(z-z_0)/\zeta\}\rho(x,y,z)\right|^2 , \quad (19)$$

where (G_x,G_y) is the scattering vector parallel to the surface. We have chosen the lowest reciprocal lattice vector of the projection of the fcc lattice onto a (110) plane. The scattering depth ζ depends on the incident angle α_i and the exit angle α_f:

$$\zeta=\frac{\zeta_0}{s_i(\alpha_i)+s_i(\alpha_f)} , \quad (20)$$

with

$$s_i(\alpha)\equiv\frac{1}{\sqrt{2}\alpha_c}[\alpha_c^2-\sin^2\alpha+\sqrt{(\alpha_c^2-\sin^2\alpha)^2+4b}\,]^{1/2} , \quad (21)$$

α_c being the critical angle for total reflection and b an extinction coefficient. The phase of the evanescent wave in z direction is given by $\kappa=[s_r(\alpha_i)+s_r(\alpha_f)]/\zeta_0$, where

$$s_r(\alpha)\equiv\frac{1}{\sqrt{2}\alpha_c}[\sin^2\alpha-\alpha_c^2+\sqrt{(\alpha_c^2-\sin^2\alpha)^2+4b^2}\,]^{1/2} . \quad (22)$$

The quantity

$$\zeta_0=\frac{c}{e}\left|\frac{m_e\varepsilon_0}{\rho Z}\right|^{1/2}=\frac{\lambda}{2\pi\alpha_c} \quad (23)$$

relates the critical angle to the x-ray wavelength λ. Z is the charge number of the atoms and m_e the electron mass. For xenon ($Z=54$, $\sigma=4.07$ Å, $\zeta_0=199\sigma$) we find $\alpha_c=30$ mrad for $\lambda=1.55$ Å. Taking $\rho=0.8\sigma^{-3}$, $\alpha_i=29$ mrad, $b=10^{-5}$, and defining z_0 by $\rho^{\perp}(z_0)=0.4\bar{\sigma}^{-3}$ we evaluate Eq. (19) by inserting the full three-dimensional density profile. The amplitudes in Fig. 8 depend significantly on the width of the liquid film. The width of the interface between liquid film and solid is reflected by the shape of the left wings of the curves.

VI. CONCLUSIONS

We examined wetting phenomena and interfaces in Lennard-Jones and hard-sphere fluids in the framework of the WDA density functional. We computed surface tensions as well as interfacial density profiles and studied, in particular, the anisotropic onset of surface melting on rare gas crystals. On the technical side we employed the method of simulated quenching which facilitates an essentially unconstrained minimization of the free energy functional. The comparison of our results with those of previous constrained variational calculations and with simulation data leads us to conclude that the effort of free minimization is indispensable for producing accurate results on interfacial structures within a density functional approach.

In the theory of fluids the hard-sphere model is usually invoked as a convenient albeit idealized reference system. However, sterically stabilized colloidal suspensions provide a concrete example of a hard-sphere fluid and even offer the chance to investigate interfacial features on a supramolecular scale with optical means.

Our study of surface melting was restricted to planar interfaces with the advantage that the systems considered had to be large enough in one dimension only. In principle, the present theory also applies to grain boundary and edge melting. To address those problems, the system must be sufficiently large in two dimensions and the storage capacity required for reasonable grid resolution is at the limit of present-day computers.

Finally, we should not conceal that the attractive part of the pair potential is treated in a physically motivated but quantitatively rather crude fashion. The current approximation is expected to affect mainly the structure of the interfacial film at its gas side. An improved modeling of the attractive interaction is clearly an important open problem for future work.

ACKNOWLEDGMENTS

This work as supported by the Bundesministerium für Forschung und Technologie (BMFT) under Contract No. 03-WA3LMU.

[1] D. P. Woodruff, *The Solid-Liquid Interface* (Cambridge University Press, Cambridge, England, 1973).

[2] H. van Beijeren and I. Nolden, in *Structure and Dynamics of Surfaces II*, edited by W. Schommers and P. van Blanckenhagen, Topics in Current Physics Vol. 43 (Springer, Berlin, 1987), p. 85.

[3] S. Dietrich, in *Phase Transitions and Critical Phenomena*, edited by C. Domb and J. L. Lebowitz (Academic, Lon-

don, 1987), Vol. 12, p. 1.
[4] H. Dosch, *Critical Phenomena at Surfaces and Interfaces,* Springer Tracts in Modern Physics Vol. 126 (Springer, Berlin, 1992).
[5] H. Löwen, Phys. Rep. **237**, 249 (1994).
[6] D. W. Oxtoby, in *Liquids, Freezing and the Glass Transition,* edited by J. P. Hansen, D. Levesque, and J. Zinn-Justin (North-Holland, Amsterdam, 1991).
[7] Y. Singh, Phys. Rep. **207**, 351 (1991).
[8] R. Evans, in *Fundamentals of Inhomogeneous Fluids,* edited by D. Henderson (Wiley, New York, 1992).
[9] W. A. Curtin and N. W. Ashcroft, Phys. Rev. A **32**, 2909 (1985).
[10] W. A. Curtin and N. W. Ashcroft, Phys. Rev. Lett. **56**, 2775 (1986); **57**, 1192(E) (1986).
[11] A. D. J. Haymet and D. W. Oxtoby, J. Chem Phys. **74**, 2559 (1981); D. W. Oxtoby and A. D. J. Haymet, *ibid.* **76**, 6262 (1982).
[12] H. Löwen, T. Beier, and H. Wagner, Europhys. Lett. **9**, 791 (1989); Z. Phys. B **79**, 109 (1990).
[13] W. E. McMullen and D. W. Oxtoby, J. Chem. Phys. **88**, 1967 (1988).
[14] R. Ohnesorge, H. Löwen, and H. Wagner, Phys. Rev. A **43**, 2870 (1991).
[15] W. A. Curtin, Phys. Rev. Lett. **59**, 1228 (1987).
[16] W. A. Curtin, Phys. Rev. B **39**, 6775 (1989).
[17] T. A. Cherepanova and A. V. Stekolnikov, J. Cryst. Growth **99**, 88 (1990).
[18] Different choices for the kernel of the double integral could be imagined: $V_a(r)$ might be given by the Barker-Henderson ansatz [32], the step function may have a different cutoff or even be replaced by a pair correlation function $g(r)$ at an effective density [48]. All these modifications do not lead to more realistic results.
[19] P. Tarazona, Mol. Phys. **52**, 81 (1984).
[20] J. F. Lutsko and M. Baus, Phys. Rev. A **41**, 6647 (1990).
[21] A. Denton and N. W. Ashcroft, Phys. Rev. A **39**, 4701 (1989).
[22] R. Leidl and H. Wagner, J. Chem. Phys. **98**, 4142 (1993).
[23] D. W. Marr and A. P. Gast, Phys. Rev. E **47**, 1212 (1993).
[24] D. J. Courtemanche and F. van Swol, Phys. Rev. Lett. **69**, 2078 (1992); D. J. Courtemanche, T. A. Pasmore, and F. van Swol, Mol. Phys. **80**, 861 (1993).
[25] H. Löwen, R. Ohnesorge, and H. Wagner, Ber. Bunsenges. Phys. Chem. **98**, 303 (1994).
[26] N. D. Mermin, Phys. Rev. **5**, A1441 (1965).
[27] J. P. Hansen and I. R. McDonald, *Theory of Simple Liquids,* 2nd ed. (Academic, London, 1986).
[28] A similar quadratic density expansion was also used by Tarazona [36] who expanded $w(r,\rho)$ around $\rho^*=0$. Since we have chosen a higher ρ^* we get a better representation of $w(r,\rho)$ for high densities relevant for the solid-fluid transition.
[29] R. Ohnesorge, H. Löwen, and H. Wagner, Europhys. Lett. **22**, 245 (1993).
[30] S. M. Foiles and N. W. Ashcroft, J. Chem. Phys. **75**, 3594 (1981).
[31] J. D. Weeks, D. Chandler, and H. C. Anderson, J. Chem. Phys. **54**, 5237 (1971).
[32] J. A. Barker and D. Henderson, J. Chem. Phys. **47**, 4714 (1967).
[33] L. Verlet and J. J. Weis, Phys. Rev. A **5**, 939 (1972).
[34] J. P. Hansen and L. Verlet, Phys. Rev. **184**, 151 (1969).
[35] In practice it is important not to use just one single mass m but to introduce a diagonal mass tensor and make an appropriate choice for its elements.
[36] P. Tarazona, Phys. Rev. A **31**, 2672 (1985).
[37] I. Z. Fisher, *Statistical Theory of Liquids* (University of Chicago Press, Chicago, 1964).
[38] J. A. Barker and D. Henderson, Rev. Mod. Phys. **48**, 619 (1976).
[39] D. M. Zhu and J. G. Dash, Phys. Rev. Lett. **57**, 2959 (1986); **60**, 432 (1988).
[40] A. Lied, H. Dosch, and Y. H. Bilgram, Phys. Rev. Lett. **72**, 3554 (1994).
[41] P. von Blanckenhagen, Ber. Bunsenges. Phys. Chem. **98**, 312 (1994).
[42] V. Pontikis and P. Sindzingre, Phys. Scr. **T19**, 375 (1987).
[43] J. M. Gay, cited in J. G. Dash, Contemp. Phys. **30**, 89 (1989).
[44] R. Evans, J. R. Henderson, D. C. Hoyle, A. O. Parry, and Z. A. Sabeur, Mol. Phys. **80**, 755 (1993).
[45] J. Q. Broughton and G. H. Gilmer, J. Chem. Phys. **84**, 5759 (1986).
[46] M. J. P. Nijmeijer, A. F. Bakker, C. Bruin, and J. H. Sikkenk, J. Chem. Phys. **89**, 1319 (1988).
[47] W. G. Hoover and F. Ree, J. Chem. Phys. **49**, 3609 (1968).
[48] L. Mederos, G. Navascues, and P. Tarazona, Phys. Rev. E **47**, 4284 (1993).

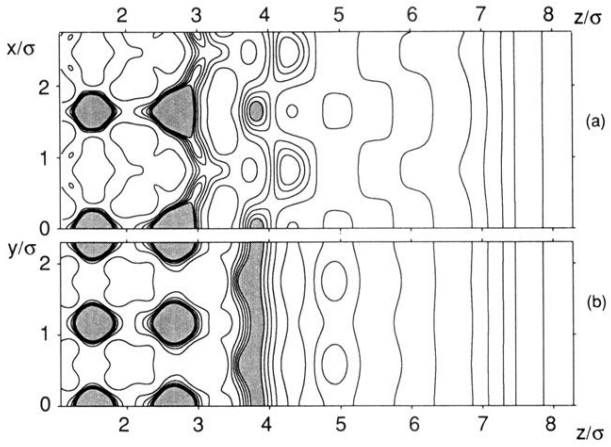

FIG. 6. (110) surface of a LJ crystal at $\tau = 10^{-4}$: Contour plots of the density in a $(1\bar{1}0)$ plane (a) and a (001) plane (b). Both planes are normal to the surface and hit the lattice sites. Lines correspond to densities $\rho\sigma^3 = 0.05 + n0.25$, $n = 0, \ldots, 6$. The shaded areas correspond to $\rho\sigma^3 > 1.55$.